Engineering Geology 114 (2010) 298–311

Contents lists available at ScienceDirect

Engineering Geology

journal homepage: www.elsevier.com/locate/enggeo

Mean particle size prediction in rock blast fragmentation using neural networks

P.H.S.W. Kulatilake [a,*], Wu Qiong [b], T. Hudaverdi [c,d], C. Kuzu [c]

[a] Geological Engineering Program, Department of Materials Science and Engineering, University of Arizona, Tucson, Arizona, 85721, USA
[b] Faculty of Engineering, China University of Geosciences, Wuhan, 430074, China
[c] Department of Mining Engineering, Istanbul Technical University, Maslak, Istanbul, 34469, Turkey
[d] Geological Engineering Program, University of Arizona, Tucson, AZ, 85721, USA

ARTICLE INFO

Article history:
Received 21 January 2010
Received in revised form 2 May 2010
Accepted 15 May 2010
Available online 14 June 2010

Keywords:
Blasting
Fragmentation
Cluster analysis
Discriminant analysis
Neural networks
Rock mass

ABSTRACT

Multivariate analysis procedures and a neural network methodology are used to predict mean particle size resulting from rock blast fragmentation. A blast data base developed in a previous study is used in the current study. The data base consists of blast design parameters, explosive parameters, modulus of elasticity and in-situ block size. In the same previous study a hierarchical cluster analysis was used to separate the blast data into two different groups of similarity based on the intact rock stiffness. In the same study the group memberships were confirmed by the discriminant analysis. A part of this blast data was used in this study to train a single-hidden layer back-propagation neural network model to predict mean particle size resulting from blast fragmentation for each of the obtained similarity groups. The mean particle size was considered to be a function of seven independent parameters. Four learning algorithms were considered to train neural network models. Levenberg–Marquardt algorithm turned out to be the best one providing the highest stability and maximum learning speed. An extensive analysis was performed to estimate the optimum value for the number of units for the hidden layer for each of the obtained similarity groups. The blast data that were not used for training are used to validate the trained neural network models. For the same two similarity groups, multivariate regression models were also developed to predict mean particle size. Capability of the developed neural network models as well as multivariate regression models is determined by comparing predictions with measured mean particle size values and predictions based on one of the most applied fragmentation prediction models appearing in the blasting literature. Prediction capability of the trained neural network models as well as multivariate regression models was found to be strong and better than the existing most applied fragmentation prediction model. Diversity of the blasts data used is one of the most important aspects of the developed models. The developed neural network models and multivariate regression analysis models are suitable for practical use at mines.

1. Introduction

Control of the particle size distribution of a muckpile after blasting is always an important subject for mining industry. Blasting has a significant impact on downstream processes of mining such as loading, crushing and grinding. Improvement of blasting results provides increase in loader and excavator productivity due to increased diggability capacity, and increased bucket and truck fill factors. Suitable and uniform particle size distribution results increase in crusher and mill throughput and decrease in energy consumption in size reduction process. Mckenzie (1966) found, in the studies at Quebec Cartier Mines, that the efficiency of all the subsystems of mining is dependent on the fragmentation. Today, researchers suggest 'mine to mill' blasting approach that is defined as optimization of the blast design to maximize the overall profitability rather than individual operations (Kanchibotla et al., 1999; Grundstrom et al., 2001). Additionally, uniform particle size distribution also eliminates the need of the secondary blasting of the big boulders.

Several studies have been conducted on blastability and prediction of fragmentation. The term blastability refers to the ease with which a rock mass can be fragmented by blasting and is closely related to fragmentation. The parameters that determine fragmentation by blasting may be divided into four groups: (a) Blast design parameters; (b) explosive parameters; (c) rock mass structure parameters; and (d) intact rock and discontinuity physical and mechanical properties. Burden, spacing between boreholes, bench height, drill-hole diameter, hole length, charge depth, stem height, subdrilling, drilling pattern (square or staggered), hole inclination (vertical or inclined), blasting direction and blasting sequence (instantaneous or delayed) are all blast design parameters. All these parameters are controllable. Fig. 1 shows most of the blast design parameters used in a bench blast. The diameter of the drill hole (D) is the most important parameter for any blast design. It influences the selection of all other parameters. Burden (B) is the distance of the blast hole from the free face. Spacing

* Corresponding author. Tel.: +1 520 621 6064; fax: +1 520 621 8059.
E-mail address: kulatila@u.arizona.edu (P.H.S.W. Kulatilake).

0013-7952/$ – see front matter
doi:10.1016/j.enggeo.2010.05.008

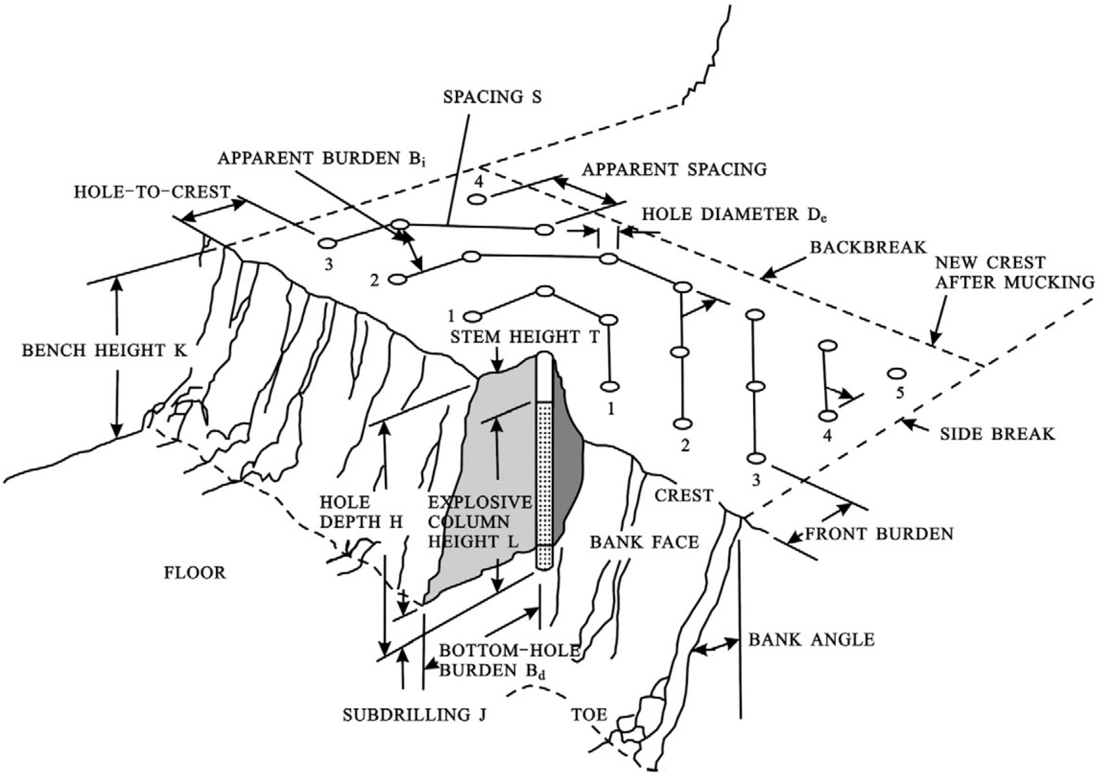

Fig. 1. Blast design parameter terminology.
Ash, 1963.

(S) is the distance between two consecutive holes fired together in the delay period. The hole is generally drilled slightly below the floor level to obtain a clean breakage. This total length of the hole is known as hole length (H). The extra length of the hole below the floor or the grade level is called the subdrilling. Part of the drill hole at the top is not filled with explosives. This length is known as stemming height (T). Some inert material, such as drill cuttings, sand, crushed stone, etc., are used as stemming to contain the explosive gases in the hole for a slightly longer time to increase rock fracturing. The second group consists of explosive parameters. Explosive type (Anfo, water gel, emulsion or dynamite), its density (changes between 0.80 and 1.60 g/cm^3), strength, resistivity and specific charge (kg Anfo/m^3) are explosive parameters. All these parameters are also controllable. The third group consists of rock mass structure parameters. Number of discontinuity sets, orientation, size, spacing and intensity distributions of each discontinuity set belong to the third group. Physical and mechanical properties of the intact rock and discontinuities belong to the fourth group. Density, dynamic compressive strength, dynamic tensile strength, shear strength, dynamic elastic properties, hardness, durability, mineral composition and grain size of intact rock, and strength, deformability, roughness and infilling material properties of discontinuities belong to the fourth group. The parameters of the third and fourth groups are uncontrollable.

The parameters of the aforementioned 4 groups should be considered together to explain fragmentation process. Because a large number of parameters influence fragmentation distribution, it is obvious that the fragmentation process is extremely complex and thus it is an extremely challenging task to develop models to predict fragmentation distribution. Therefore, even though some of the fragmentation prediction models that appear in the literature have contributed to improving the state-of-the-art on the subject, none of them include all the important parameters. In some of the available prediction models crude, highly simplified or inappropriate procedures have been used in estimating rock mass fracture geometry parameters. Inappropriate distributions have been used to represent joint orientation. Corrections for sampling biases have not been applied in modeling joint size, joint orientation and joint intensity. Estimation of fracture spacing has been described in a highly vague manner. It is important to note that spacing of a fracture set changes with the direction and the correct spacing is obtained in the direction perpendicular to the fracture plane. In some of the blast fragmentation papers, RQD is used as a parameter. It is important to note that RQD changes with the direction and thus infinite many values exist for RQD for the same rock mass. In-situ block size estimation has not been done in a comprehensive manner. Therefore, it is important to use better and accurate procedures in estimating rock mass fracture geometry parameters in developing rock blast fragmentation data bases in the future. Such quality data bases should then be used to improve the existing models or to develop new models to predict rock blast fragmentation distribution.

Because the blast fragmentation distribution depends on many parameters, and the process is highly complex due to the heterogeneity and anisotropy of a discontinuous rock mass system, it is impossible to derive an equation for fragmentation distribution purely from theoretical and mechanistic reasoning. In such situations, empirical approaches are used incorporating case history data along with statistical based procedures in developing prediction equations for complex geotechnical processes. Multivariate regression analysis has been used to develop fragmentation prediction models (Chakraborty et al., 2004; Hudaverdi et al., 2010). However, capturing of high non-linearity incorporating many parameters is a difficult task with multivariate regression analysis.

Neural computing (Eberhart and Dobbins, 1990) attempts to emulate the functions of the mammalian brain, thus mimicking thought processes. Work on artificial neural networks (ANNs), commonly referred to as "neural networks," has been motivated right from its inception by the recognition that the human brain computes in an entirely different way from the conventional digital computer. The brain is a highly complex, nonlinear, and parallel computer. It has the capability to perform certain computations (e.g., pattern recognition, perception, and motor control) many times faster than the fastest digital computer in existence today. In its most general form, a neural network is a machine that is designed to model the way in which the brain performs a particular task or function of interest; the network is usually implemented by using electronic components or is simulated in software on a digital computer. To achieve good performance, neural networks employ a massive interconnection of simple computing units referred to as "neurons" or "processing units." A neural network can be defined as a massively parallel distributed processor made up of neurons, which has a natural propensity for storing experimental knowledge and making it available for use. It resembles the brain in two respects: 1. Knowledge is acquired by the network from its environment through a learning process; and 2. Interneuron connection strengths, known as synaptic weights, are used to store the acquired knowledge. The procedure used to perform learning process is called a "learning algorithm" and the function of it is to modify the synaptic weights of the network in an orderly fashion to attain a desired design objective. It is apparent that a neural network derives its computing power through, first, its massively parallel distributed structure and second, its ability to learn and therefore generalize. Generalization refers to the neural network producing reasonable outputs for inputs not encountered during training (learning) process. These two information processing capabilities make it possible for neural networks to solve complex (large scale) problems that are currently intractable. The use of neural networks offers the following useful properties and capabilities: 1. *Nonlinearity*; 2. *Input–Output Mapping*: Each example consists of a unique input signal and a corresponding desired response. The network is presented with a randomly picked training sample from a set and the synaptic weights of the network are modified to minimize the difference between the desired response and the actual response of the network produced by the input signal in accordance with an appropriate statistical criterion. The training of the network is repeated for many examples in the set until the network reaches a steady state where there are no further significant changes in the synaptic weights. Such a trained neural network model has a good generalization capability; 3. *Adaptivity*: Neural networks have a built-in capability to changes in the surrounding environment. In particular, a neural network trained to operate in a specific environment can be easily retrained to deal with minor changes in the operating environmental conditions; 4. *Contextual Information*: Knowledge is represented by the very structure and activation state of a neural network. Every neuron in the network is potentially affected by the global activity of all other neurons in the network. Consequently, contextual information is dealt with naturally by a neural network; and 5. *Fault Tolerance*: A neural network, implemented in hardware form, has the potential to be inherently fault tolerant, or capable of robust computation, in the sense that its performance degrades gracefully under adverse operating conditions.

Due to its excellent ability of non-linear pattern recognition, generalization, self-organization and self-learning, the Artificial Neural Network Approach (ANNA) has been proved to be of widespread utility in engineering and is steadily advancing into diverse areas as material sciences (Li et al., 2006), voice recognition, loan-risk assessment, stock market analysis, box office revenue forecasting (Zhang et al., 2009) and military target discrimination. In geosciences and geo-engineering, neural networks have been applied in rock mechanics and rock engineering (Zhang et al., 1991; Ghaboussi, 1992; Lee and Sterling, 1992), soil engineering (Kung et al., 2007), well-log and well-test interpretation (Rogers et al., 1992; Al-Kaabl and Lee, 1993), seismic and satellite image processing (de Groot, 1993; Penn et al., 1993), groundwater characterization and remediation (Rizzo and Doughery, 1994; Rogers and Dowla, 1994), earthquake intensity prediction (Tung et al., 1994), oil reservoir prediction (Yu et al., 2008) and conductive fracture identification (Thomas and La Pointe, 1995). Neural network approach (NNA) is highly suitable for systems with highly non-linear complex relations between input and output parameters that are difficult to develop through physical reasoning and mathematical modeling. Linking between the rock blast mean fragment size and the blast design parameters, explosive parameters, rock mass structure parameters, and intact rock and discontinuity physical and mechanical properties is a very complex, non-linear process. Therefore, NNA will be highly suitable to relate the mean fragment size to the aforementioned blast related parameters belonging to the four groups. Application of NNA to predict rock blast mean fragmentation size is described in this paper.

2. Literature review

The importance of in-situ joints and fractures on the degree of fragmentation has been explained by Ghosh et al. (1990) and Mojtabai et al. (1990). Twelve production blasts in a quarry in Java have shown a large influence of tightly spaced porous bands, which were weaker than the host rock, on the fragmentation distribution (Ouchterlony et al., 1990). Chakraborty et al. (1994) have reported that the joint orientations can considerably influence the average fragment size and shape. Through three case studies, Pal Roy (1995) has shown that the new cracking directions in rock masses due to blasting depend on the existing discontinuity orientation directions.

Hagan (1995) has concluded that the results of rock blasting are affected more by rock properties than by any other variables. He also has stated that as the mean spacing between the joints, fissures or the cracks decreases, the importance of rock material strength decreases while that of the rock mass strength increases. In addition he states that in a rock mass with widely spaced joints, the blasts are required to create many new cracks. In a closely fissured rock mass, on the other hand, generation of new cracks is not needed and the fragmentation is achieved by the explosion gas pressure which opens the joints to transform a large rock mass into several loose blocks. According to him, the generation of new cracks is influenced by both dynamic compressive and dynamic tensile strength of rock mass. He also has commented that the blasting efficiency is affected to a lesser degree by the internal friction, grain size and porosity compared to rock strength.

Aler et al. (1996) have evaluated blasting efficiency through a comparison between block size of the rock mass resulting from existing fractures and the fragmentation size distribution resulting from blasting. Image analysis techniques have been applied to randomly taken photos to derive the blast fragmentation distribution. The procedures have been illustrated by applying to several case histories. Through three case studies, Ozcelik (1998) has shown influence of rock mass structure parameters on blast fragmentation distribution. Jhanwar et al. (2000) using a case study have shown the influence of in-situ block size on fragmentation distribution. In-situ block size has been estimated using a simple method known as volumetric joint count.

Castro et al. (1998) created a blasting index for exploitation of aggregates. They estimated strength parameters and structural parameters of the rock mass. A blasting index was developed using linear discriminant analysis. This index provided a single value that contains all structural and strength properties to evaluate blasting of the rock mass.

Latham and Lu (1999) have considered intact rock properties and the discontinuity structure of a rock mass as the most important variables influencing blasting results. This influence has been considered to be a composite intrinsic property of a rock mass and is referred to as the blastability of a rock mass. A blastability index has been developed using intact rock properties and discontinuity structure parameters based on a rock engineering systems approach.

A case study has been given to illustrate the application of the developed procedure.

Chakraborty et al. (2004) have performed detailed investigations on overburden blasting and fragmentation in three large opencast coal mines. RQD has been used to represent all the rock mass structure parameters. Based on RQD, investigated rock masses have been separated into jointed and massive categories. Stepwise multiple linear regression analysis have been carried out separately for jointed and massive formations keeping the observed mean fragment size as the dependent variable and various rock mass properties, explosive properties, blast design parameters, drilling error and the firing sequence as independent variables. The degree of dominance of various influencing parameters has been determined as a result. Based on the results, suggestions have been put forward as remedial measures to improve fragmentation in massive and jointed formations. However, some influencing parameters have not been considered either due to non-availability of data or non-availability of sufficient number of blasts.

Hamdi and Du Mouza (2005) have applied a cluster analysis procedure to classify rock masses using several discontinuity geometry and rock matrix properties. Several parameters assessing the density (specific surface), the interconnectivity (interconnectivity index) and the anisotropy (anisotropy index and anisotropy vector) of the discontinuity network as well as the 3D fractal dimension of the rock mass have been introduced and evaluated for three sites. The rock matrix microstructure has been characterized by the means of the experimental determination of several mechanical and physical parameters. Laboratory measurements performed on cores coming from the blasted blocks have been used for fine characterization of the microstructure status.

Several methods have been being used in the literature to measure the fragmentation distribution. Digital image processing technique using sophisticated software and hardware is the latest fragmentation analysis tool (Hall and Brunton, 2002; Latham et al., 2003; Sanchidrian et al., 2007; Gheibie et al., 2009) and has replaced in many cases the conventional methods like visual analysis, photographic, photogrammetry, boulder count or sieve analysis techniques which have inherent problems. Because muck piles are large, use of conventional methods is tedious and time consuming and thus not practicable for measurement of blast fragmentation distribution of muck piles. The digital image processing method includes image capturing of muck pile, scaling the image, filtering the image, segmentation of image, binary image manipulation, measurement and stereometric interpretation. The method is quick. However, many problems exist with this technique too. The individual rock fragments in the image must be delineated. Problems with non-uniform lighting, shadows and the large range of fragment sizes make delineation very difficult using standard edge detection routines. Other problem is correct extraction of three dimensional information from the two-dimensional images for which assumption and site specific calibration for the third dimension are to be made from the two-dimensional images. Further, a correction is to be made for overlapping of fragments or estimating the fines which may not be detected individually. Ouchterlony et al. (1990) have observed major discrepancies between sieving and digital image analysis results. Digital image analysis results have produced more fines. The computer treats all un-digitized voids between the fragments as fines. This may be another source of error of digital image analysis method. Finally, the wide variations in size may require different scales for calibration. Rustan (1998) and Chakraborty et al. (2004) have summarized the capabilities of various image analysis software developed world-wide for blast fragmentation assessment.

Kuznetsov (1973) has suggested the following empirical equation to predict the mean fragmentation size resulting from rock blasting:

$$X_{50} = A(V/Q)^{0.8}Q^{0.167} \tag{1}$$

In Eq. (1): X_{50} is mean fragment size (cm); 'A' is a rock factor (7 for medium rock, 10 for hard highly fissured rock, and 13 for hard weakly fissured rocks); V is rock volume (m^3); Q is mass of explosive per blast hole (kg). Kuznetsov also has suggested to use Rosin–Rammler equation (Rosin and Rammler, 1933) given below to estimate the complete fragmentation distribution resulting from rock blasting:

$$Y = \exp(X/X_c)^r \tag{2}$$

In Eq. (2), $Y =$ Proportion of the material larger than X, $X_c =$ characteristic size $= X_{50}$ and $r =$ uniformity exponent. Even though Schumann Distribution (Schuhmann, 1959) and Swebrec equation (Nie and Rustan, 1987) are also suggested in the literature to predict the complete fragmentation distribution, Rosin–Rammler equation seems to be the most popular one.

It was experienced by many that the rock mass categories defined by Kuznetsov (1973) are very wide and need more precision. Cunningham (1983, 1987) modified the Kuznetsov's equation to estimate the mean fragment size and used the Rosin–Rammler distribution to describe the entire size distribution. The uniformity exponent of Rosin–Rammler distribution was estimated as a function of blast design parameters. Rock factor "A" in Kuznetsov's equation was estimated incorporating the blasting index, BI of Lilly (1986). The final equation suggested by Cunningham, known as Kuz–Ram model, can be given as follows:

$$X_{50} = A \times (V/Q)^{0.8} \times Q^{0.167} \times (E/115)^{-0.633} \tag{3}$$

where,

$$A = 0.06 \times BI \tag{4}$$

and

$$BI = 0.5 \times (RMD + JPS + JPO + RDI + S) \tag{5}$$

In Eq. (3), E is relative weight strength of explosive (Anfo = 100) and $V = BSH$ where $B =$ burden (m), $S =$ blast hole spacing (m) and $H =$ bench height (m). In Eq. (5): RMD is rock mass description (powdery or friable = 10, blocky = 20 and massive = 50); JPS is joint plane spacing (close < 0.1 m = 10, 0.1–1.0 = 20, > 1.0 = 50); JPO is joint plane orientation (horizontal = 10, dip out face = 20, strike normal to face = 30, dip into face = 40) and RDI is rock density influence equal to $25d - 50$, where d is density and S is rock strength, equal to 0.05 UCS, where UCS is uniaxial compressive strength. Even though a few other equations such as SveDefo's fragmentation model (Hjelmberg, 1983) and the model of Kou and Rustan (1993) are also available in the literature to estimate mean fragmentation size, Kuz–Ram model seems to be the most popular one.

Research at the JKMRC, Australia and elsewhere has demonstrated that the Kuz–Ram model underestimates the contribution of fines in the fragment size distribution. Hall and Brunton (2002) claim that the JKMRC model provides better prediction than Kuz–Ram model due to improved estimation of the fines to intermediate size (<100 mm) of the fragmentation distribution. The JKMRC model calculates the coarse and fines distributions independently. JKMRC uses Kuz–Ram model to calculate the course fraction.

In a previous study conducted by the third, first and fourth authors of this paper (Hudaverdi et al., 2010), many blasts performed in different parts of the world and reported in the literature were carefully analyzed and put together to create a blast data base to develop fragmentation prediction models. In the data base, the burden, spacing between holes, stemming, bench height and hole diameter are used to represent blast design parameters. Specific charge is used as the explosive parameter that represents explosive distribution in rock. All blasts in the database were performed using Anfo. Therefore, there was no need to use any parameter related to explosive type. Because the data base was large and diverse, it turned out to be a difficult assignment to find common intact rock and rock mass parameters for all the selected blast data to use in developing fragmentation distribution models. On the other hand, it was possible to find in-situ block size for all the blasts in the data base. Therefore, in-situ block size which is accepted as one of the key parameters of the fragmentation process was used to represent rock mass structure in the data base. With respect to intact rock, the modulus of elasticity turned out to be the most common parameter available for all the blasts and was used to represent intact rock properties in the data base. The cluster analysis was performed on this data to separate the blast data into two different similarity groups. The main difference between the two groups was found to be the modulus of elasticity value. The data belonging to the two groups are given in Tables 1 and 2, respectively. The mean elastic modulus values are 51.14 and 17.99 for Groups 1 and 2, respectively. Group memberships were then analyzed and confirmed by the discriminant analysis. In this paper, a part of the blast data is used to train neural network models for each of the obtained similarity groups. The blast data that are not used for training are used to validate the trained neural network models.

3. Used blast database

This section covers the blast data base developed by Hudaverdi et al. (2010). The data compiled from previous blasts conducted in various parts of the world were combined with blast data collected from the quarries near Istanbul city to create the blast data base. A total of 91 blasts shown in Tables 1 and 2 were evaluated to form a blast database. The blasts shown by symbols 'Rc,' 'En' and 'Ru' in Table 1 were collected from Aler et al. (1996) and Hamdi et al. (2001) research conducted at the Enusa and Reocin mines which are located in Spain. The Enusa Mine is an open-pit uranium mine in a schistose and is a moderately to heavily folded formation. The Reocin mine is an open-pit and underground zinc mine. The Reocin underground mine also applies bench blasting technique. The bench height in the Enusa mine was 6 m. The bench height in the Reocin mine was between 9 and 11 m. the bench height in the Reocin underground mine was 18 m. Hole diameters for the Enusa and Reocin mines were 165 mm and 229 mm, respectively.

The blasts shown by symbol 'Mg' in Table 1 were performed in the Murgul Copper Mine (Hudaverdi, 2004). The Murgul Copper Mine is a large open-pit mine located in the northeastern Turkey. The drill-hole diameter applied was 165 mm. The bench height was 12 m. The burden distance varied between 4.5 and 5 m. The spacing between holes was 4.5–5.5 m. The rock formation was mainly dacite and altered dacite.

Table 1
Blast data belonging to Group 1.

	S/B	H/B	B/D	T/B	Pf (kg/m^3)	X_B (m)	E (GPa)	X_{50} (m)
En1	1.24	1.33	27.27	0.78	0.48	0.58	60.00	0.37
En2	1.24	1.33	27.27	0.78	0.48	0.58	60.00	0.37
En3	1.24	1.33	27.27	0.78	0.48	1.08	60.00	0.33
En4	1.24	1.33	27.27	0.78	0.48	1.11	60.00	0.42
En5	1.24	1.33	27.27	0.78	0.48	1.08	60.00	0.46
En6	1.24	1.33	27.27	1.17	0.27	1.08	60.00	0.37
En7	1.24	1.33	27.27	1.06	0.33	1.08	60.00	0.64
En8	1.24	1.33	27.27	0.91	0.41	1.11	60.00	0.42
En9	1.24	1.33	27.27	0.91	0.41	1.11	60.00	0.26
En10	1.24	1.33	27.27	0.99	0.36	1.08	60.00	0.42
En11	1.24	1.33	27.27	1.06	0.33	1.11	60.00	0.31
En12	1.24	1.33	27.27	1.06	0.33	1.11	60.00	0.38
Rc2	1.17	1.50	26.20	1.12	0.30	0.68	45.00	0.48
Rc3	1.17	1.58	26.20	1.22	0.28	0.68	45.00	0.48
Rc4	1,17	1,96	26,20	1,30	0,34	1,56	45,00	0,75
Rc5	1.17	1.75	26.20	1.31	0.29	1.56	45.00	0.96
Rc6	1.17	1.75	26.20	1.16	0.36	1.56	45.00	0.76
Rc7	1.17	1.67	26.20	1.22	0.31	1.80	45.00	0.53
Rc8	1.17	1.83	26.20	1.34	0.30	1.80	45.00	0.56
Rc9	1.17	1.83	26.20	1.29	0.32	1.80	45.00	0.74
Rc10	1.17	1.83	26.20	1.23	0.35	1.80	45.00	0.44
Mg1	1.00	2.67	27.27	0.89	0.75	0.83	50.00	0.23
Mg2	1.00	2.67	27.27	0.89	0.75	0.78	50.00	0.25
Mg3	1.00	2.40	30.30	0.80	0.61	1.02	50.00	0.27
Mg4	1.00	2.40	30.30	0.80	0.61	0.75	50.00	0.30
Mg5	1.10	2.40	30.30	0.80	0.55	1.18	50.00	0.38
Mg6	1.10	2.40	30.30	0.80	0.55	1.24	50.00	0.37
Mg7	1.10	2.40	30.30	0.80	0.55	1.33	50.00	0.38
Ru1	1.13	5.00	39.47	1.93	0.31	2.00	45.00	0.64
Ru2	1.20	6.00	32.89	3.67	0.30	2.00	45.00	0.54
Ru3	1.20	6.00	32.89	3.70	0.30	2.00	45.00	0.51
Ru4	1.20	6.00	32.89	4.67	0.22	2.00	45.00	0.64
Ru5	1.20	6.00	32.89	3.11	0.35	2.00	45.00	0.54
Ru6	1.20	6.00	32.89	3.22	0.34	2.00	45.00	0.69

Table 2
Blast data belonging to Group 2.

	S/B	H/B	B/D	T/B	Pf (kg/m^3)	X_B (m)	E (GPa)	X_{50} (m)
Mr1	1.20	6.00	32.89	0.80	0.49	1.67	32.00	0.17
Mr2	1.20	6.00	32.89	0.80	0.51	1.67	32.00	0.17
Mr3	1.20	6.00	32.89	0.80	0.49	1.67	32.00	0.13
Mr4	1.20	6.00	32.89	0.80	0.52	1.67	32.00	0.17
Mr5	1.20	6.00	32.89	0.80	0.42	1.67	32.00	0.13
Mr6	1.40	6.00	32.89	0.80	0.36	1.67	32.00	0.15
Mr7	1.20	6.00	32.89	0.60	0.56	1.03	32.00	0.18
Mr8	1.40	6.00	32.89	0.60	0.30	1.03	32.00	0.19
Mr9	1.40	6.00	32.89	0.60	0.35	1.03	32.00	0.16
Mr10	1.16	5.00	39.47	0.50	0.39	1.03	32.00	0.17
Mr11	1.16	5.00	39.47	0.50	0.32	1.03	32.00	0.21
Db1	1.25	3.50	20.00	1.75	0.73	1.00	9.57	0.44
Db2	1.25	5.10	20.00	1.75	0.70	1.00	9.57	0.76
Db3	1.38	3.00	20.00	1.75	0.62	1.00	9.57	0.35
Db4	1.50	5.50	20.00	1.75	0.56	1.00	9.57	0.55
Db5	1.75	4.75	20.00	1.75	0.39	1.00	9.57	0.35
Db6	1.25	4.75	20.00	1.75	0.33	1.00	9.57	0.23
Db7	1.25	5.00	20.00	1.75	0.44	1.00	9.57	0.40
Db8	1.20	2.40	25.00	1.40	0.28	0.50	9.57	0.35
Db9	1.40	3.20	25.00	1.40	0.31	0.50	9.57	0.29
Sm1	1.25	2.50	28.57	0.83	0.42	0.50	13.25	0.15
Sm2	1.25	2.50	28.57	0.83	0.42	0.50	13.25	0.19
Sm3	1.25	2.50	28.57	0.83	0.42	0.50	13.25	0.23
Sm4	1.25	2.50	28.57	0.83	0.42	1.50	13.25	0.22
Sm5	1.25	2.50	28.57	0.83	0.42	1.50	13.25	0.24
Sm6	1.25	2.50	28.57	0.83	0.42	1.50	13.25	0.26
Sm7	1.25	2.50	28.57	0.83	0.42	1.50	13.25	0.28
Ad1	1.20	4.40	28.09	1.20	0.58	0.77	16.90	0.15
Ad2	1.20	4.80	28.09	1.20	0.66	0.56	16.90	0.17
Ad3	1.20	4.80	28.09	1.20	0.72	0.29	16.90	0.14
Ad4	1.20	4.00	28.09	1.60	0.49	0.81	16.90	0.16
Ad5	1.14	6.82	24.72	1.36	0.84	1.43	16.90	0.21
Ad6	1.14	6.36	24.72	1.36	0.82	1.77	16.90	0.21
Ad7	1.25	3.50	22.47	1.25	0.75	1.03	16.90	0.15
Ad8	1.25	3.25	22.47	1.25	0.71	0.83	16.90	0.19
Ad9	1.25	3.50	22.47	1.25	0.76	1.68	16.90	0.18
Ad10	1.25	3.50	22.47	1.25	0.76	1.24	16.90	0.15
Ad11	1.14	3.18	24.72	1.14	0.69	0.67	16.90	0.14
Ad12	1.14	3.18	24.72	1.14	0.69	2.01	16.90	0.20
Ad13	1.12	2.80	28.09	1.00	0.54	0.96	16.90	0.15
Ad14	1.00	2.40	28.09	1.00	0.56	0.83	16.90	0.14
Ad15	1.10	3.75	21.74	1.00	1.02	1.64	16.90	0.15
Ad16	1.10	3.50	22.47	1.25	0.86	2.35	16.90	0.15
Ad17	1.25	3.75	17.98	1.56	1.24	1.53	16.90	0.19
Ad18	1.00	4.00	18.42	1.71	1.26	0.73	16.90	0.15
Ad19	1.00	4.00	18.42	1.71	1.26	1.47	16.90	0.17
Ad20	1.14	4.00	18.42	1.71	1.10	1.19	16.90	0.19
Ad21	1.11	4.44	18.95	1.67	1.25	1.71	16.90	0.22
Ad22	1.28	3.61	18.95	1.67	0.89	0.56	16.90	0.20
Oz1	1.00	2.83	33.71	1.00	0.48	0.45	15.00	0.27
Oz2	1.20	2.40	28.09	1.00	0.53	0.86	15.00	0.14
Oz3	1.20	2.40	28.09	1.00	0.53	0.44	15.00	0.14
Oz4	1.25	4.50	22.47	1.50	0.76	0.66	15.00	0.20
Oz5	1.11	3.33	30.34	1.11	0.47	0.47	15.00	0.17
Oz6	1.20	3.20	28.09	1.20	0.48	1.11	15.00	0.30
Oz7	1.20	2.40	28.09	1.00	0.70	0.88	15.00	0.12

The blasts shown by symbol 'Mr' was obtained from the research of Ouchterlony et al. (1990) performed in the Mrica Quarry in Indonesia. The research was a part of SveDeFo (Swedish Detonic Research Foundation) investigations on fragmentation prediction models. The rock was mainly andesite. The hole diameter was 76 mm and bench height was 10–15 m. They investigated the effect of rock mass properties and blast design parameters on blasting results. Ouchterlony compared his results with the results of the SveDeFo and Kuz–Ram prediction models.

The blasts indicated with symbol 'Sm' in Table 2 were performed in an open-pit coal mine in Soma Basin which is located in Western Turkey. Ozcelik (1998) investigated 8 blasts to explain the effect of the joint systems on fragmentation. The diameter of the blast holes was 21 cm. The burden was 5 m and spacing was 7.5 m. The bench height was 15 m. The holes were drilled in two rows. Ozcelik determined particle size distribution by image analysis software.

The blasts indicated with 'Db' symbol were performed in the Dongri–Buzurg open-pit manganese mine situated in Central India. Generally, the rock was micaceous schist and muscovite schist. The hole diameter was 100 mm and bench height was 6–11 m. The burden was between 2 and 2.5 m and spacing was between 1.8 and 3.5 m. The in-situ block size used to define the rock mass was determined by the volumetric joint count (Jhanwar et al., 2000).

The blasts shown by symbols 'Ad' and 'Oz' were performed at the Akdaglar and Ozmert Quarries of Cendere basin located in the northern Istanbul. The blasts are investigated by the third and fourth authors of this paper as a part of ongoing Istanbul Technical University Research Project entitled "the investigation of environmentally friendly blast designs for improvement of fragmentation in Istanbul region quarries." The aim of the project is to develop a fragmentation model for improvement of the productivity in Istanbul region quarries. Istanbul is a rapidly growing city. Most of the construction projects in Turkey are concentrated in Istanbul. The quarries work intensively to provide aggregate for concrete plants. Additionally, the growing city approaches the quarries. Operation of the quarries near residential areas is getting difficult day by day because of the environmental pressures. Therefore, working with high efficiency and getting desired particle size distribution resulting from blasts are a necessity. The Akdaglar quarry produces aggregate for concrete and asphalt plants. Daily capacity of the quarry is 5000 tons. The rock of the quarry is sandstone. The density of the rock is 2.70 g/cm^3. The average compressive strength is 81 MPa. The Young modulus is 16.9 GPa. Anfo was used as the column charge. The drill-hole diameter was 89 mm. The average burden applied was 2.17 m with a standard deviation of 0.35. The average spacing distance was 2.5 m. The rock of the Ozmert quarry was also sandstone. The hole diameter was 89 mm. In the Ozmert Quarry, the burden applied was 2.5 m and spacing between holes was 3 m. The particle size distribution of the blasts performed in the Cendere Basin quarries was estimated by the Wipfrag image analysis software. After each blast, multiple images were captured from different locations of the muckpile. The images were analyzed separately and the results were combined. The discontinuity properties of the rock and the apparent in-situ block size of the benches were analyzed by the Wipjoint joint analysis software. Wipjoint is also a product of the creators of the Wipfrag. Wipjoint allows users to quantify bench characteristics such as the joint orientation, spacing and block size. The images of the bench face were captured before each blast was performed at the Cendere region quarries and an average in-situ block size was determined.

Five main blast design parameters are used in the developed neural network models. They are the burden (B, m), spacing (S, m), bench height (H, m), stemming (T, m) and hole diameter (D, m). Several blasting researchers have considered blast design parameters as ratios. In this study, the blast design parameters of all the blast data are also used as ratios. The ratio of bench height to drilled burden (H/B), ratio of spacing to burden (S/B), ratio of burden to hole diameter (B/D) and ratio of stemming to burden (T/B) are the blast design parameters used. The Powder factor (Pf) has been considered as an explosive parameter. The ratio of spacing to burden is determined based on energy coverage of the bench. For square pattern, S/B ratio is 1. The mean S/B ratio of the used blast data is 1.20. Generally, the ratio of stemming to burden applied is around 1. For the used data, the mean T/B ratio is 1.27 with a standard deviation of 0.69. Low T/B ratio may cause premature release of explosive gases and result in flyrock and inefficient fragmentation. Conversely, excessive stemming length means low specific charge and may cause large boulders. Most of the blast design calculations start with burden determination. If the burden is too small, detonation gases escape to the atmosphere. Escape of the detonation gases cause noise and airblast. That means less energy is used for fragmentation. If the burden is too large, confined gases may cause ground vibrations and backbreak. The particle size of the muckpile may be coarser than expected under such a situation. The ratio of burden to hole diameter (B/D) is one of the most important parameters. Ash (1963) suggested the ratio of burden to hole diameter (B/D) as 30 for average conditions. The B/D ratio is equal to 25 for low density explosives such as Anfo. For the used data, the mean B/D ratio is 27.21 with a standard deviation of 4.77. In this study, the ratio of the bench height to burden (H/B) is used instead of the ratio of hole length to burden (L/B) used by Ash. The ratio of bench height to burden indicates the stiffness of the rock beam under blast induced stress (2004). Hustrulid (1999) indicated that the H/B ratio is 1.6 or more for most of the open-pit operations. The mean H/B ratio of the data used is 3.44 with a standard deviation of 1.64. Thus 7 parameters were used to establish fragmentation prediction models based on NNA incorporating the blast design parameters, modulus of elasticity (E, GPa) and in-situ block size (X_B, m). Table 3 shows the descriptive statistics of the parameters that were used to develop neural network based fragmentation prediction models.

4. Application of Artificial Neural Network Approach (ANNA)

4.1. Setting up and training of ANNA

The back-propagation (BP) network, a multilayer feed-forward ANNA, is perhaps the most popular network architecture today as it contains the highlights of the neural network theory, simple in structure and clear in mathematical meaning. It has been proved that any continuous function can be uniformly approximated by BP network model with only one hidden layer (Cybenko, 1989). So a single-hidden layer BP network is used in this paper to predict the mean particle size of rock fragmentation resulting from blasting. As stated previously, the mean particle size X_{50} is considered to be a function of seven independent parameters. Consequently, the parameters S/B, H/B, B/D, T/B, Pf, X_B and E are used as inputs and X_{50} as the output in the BP network model. In the literature different opinions are expressed with respect to designing the neural network structure with respect to the number of nodes and the weights to obtain accurate performance from a trained network for a given number of

Table 3
Descriptive statistics of the input parameters used to develop fragmentation prediction models.

	Minimum	Maximum	Mean	Std. deviation
S/B	1.00	1.75	1.20	0.109
H/B	1.33	6.82	3.44	1.64
B/D	17.98	39.47	27.21	4.77
T/B	0.50	4.67	1.27	0.688
Pf (kg/m^3)	0.22	1.26	0.53	0.238
X_B (m)	0.02	2.35	1.17	0.479
E (GPa)	9.57	60.00	30.74	17.72

S = Spacing; B = Burden; H = Hole depth; D = drill-hole diameter; T = Stemming height; Pf = Powder factor; X_B = Mean block size; E = Elastic modulus.

training samples. This aspect is discussed in Section 4.2. Research conducted in the past has shown that the number of hidden units has a great impact on the ANNA prediction results (Khaw et al., 1995; Maier and Dandy, 1997). Fig. 2 shows the BP network configuration used in this study assuming the optimum number of hidden units as N. Section 4.3 deals with estimation of N in great detail.

Assume the input vector of the network given in Fig. 2 as P given below in Eq. (6).

$$P = (a_1, a_2, a_3, a_4, a_5, a_6, a_7) \tag{6}$$

The expressions for input (S_j) and the output (b_j) of the jth neuron in the hidden layer are respectively given by Eqs. (7) and (8) (Ge and Sun, 2007).

$$s_j = \sum_{i=1}^{7} w_{ij} a_i - \theta_j \qquad j = 1, 2, 3, \ldots, N \tag{7}$$

$$b_j = f_1\left(s_j\right) \qquad j = 1, 2, 3, \cdots, N \tag{8}$$

$$f_1(x) = \frac{2}{1 + e^{-2x}} - 1 \tag{9}$$

In Eq. (7), w_{ij} and θ_j are the weights and thresholds respectively, between the input layer and the hidden layer. The transfer function of the hidden layer is given by Eq. (9). The input can be mapped into the output interval between −1 and 1.

The expressions for input (L_t) and the output (C_t) of the tth neuron in the output layer are respectively given by Eqs. (10) and (11) (Ge and Sun, 2007).

$$L_t = \sum_{i=1}^{N} v_{jt} b_j - \gamma_t \qquad t = 1 \tag{10}$$

$$C_t = f_2(L_t) \qquad t = 1 \tag{11}$$

$$f_2(x) = \frac{1}{1 + e^{-x}} \tag{12}$$

In Eq. (10), v_{jt} and γ_t are the weights and thresholds respectively, between the hidden layer and the output layer. The transfer function of the output layer [Eq. (12)] is of log-sigmoid type. The input can be mapped into the output interval between 0 and 1.

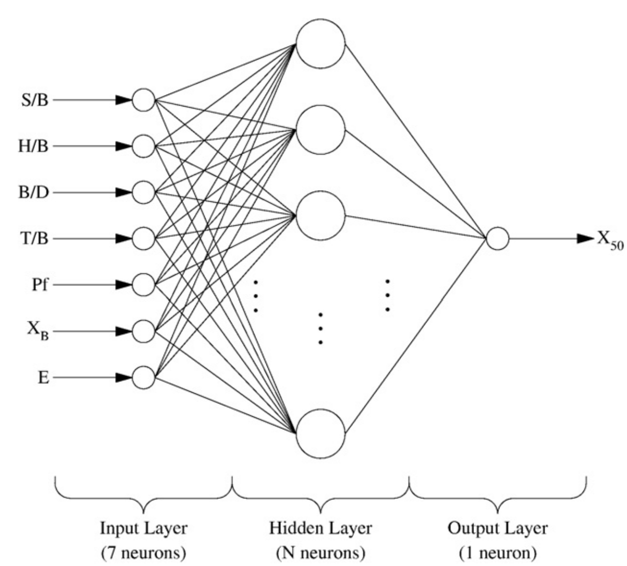

Fig. 2. The structure of a 7-N-1 BP neural network.

According to the aforementioned training rule, the information flows through the network from the input layer to the output layer via the hidden layer. The objective of the training is to adjust the aforementioned weights and thresholds to develop and estimate a complicated non-linear function between the output and input variables. The objective function given in Eq. (13) is used to obtain an optimized trained network.

$$MSE = \frac{1}{T} \sum_{t=1}^{T} (y_t - C_t)^2 \tag{13}$$

In Eq. (13), y_t is the expected output; T is the number of data sets used in the training sample. The weights and thresholds are adjusted using the gradient decreased learning method to minimize the objective function value given by Eq. (13) and thus to arrive at an optimized trained network. The adjusting functions for the weights and thresholds between the hidden layer and the output layer are given by Eqs. (14) and (15), respectively.

$$v_{jt}(m+1) = v_{jt}(m) + \alpha(y_t - C_t)C_t(1 - C_t)b_j \tag{14}$$

$$\gamma_t(m+1) = \gamma_t(m) + \alpha(y_t - C_t)C_t(1 - C_t) \tag{15}$$

In Eqs. (14) and (15), α is the learning rate between the hidden layer and the output layer ($0<\alpha<1$) and m stands for the mth adjustment. The adjusting functions for the weights and thresholds between the input layer and the hidden layer are given by Eqs. (16) and (17), respectively.

$$w_{ij}(m+1) = w_{ij}(m) + \beta\left[\sum_{t=1}^{1} (y_t - C_t)C_t(1 - C_t)v_{jt}\right] b_j\left(1 - b_j\right) a_i \tag{16}$$

$$\theta_j(m+1) = \theta_j(m) + \beta\left[\sum_{t=1}^{1} (y_t - C_t)C_t(1 - C_t)v_{jt}\right] b_j\left(1 - b_j\right) \tag{17}$$

In Eqs. (16) and (17), β is the learning rate between the input layer and the hidden layer ($0<\beta<1$). The initial values of the weights (w_{ij}, v_{jt}), thresholds (θ_j, γ_t) and the learning rates (α,β) are input automatically when "newff" function is used to create a BP network in the neural network toolbox of the Matlab software. The training of the network is stopped after it has been trained for many cycles to reach a stable *MSE* value.

As stated before, the blasting data have been divided into two groups by the value of elastic modulus. To increase the prediction precision, BP neural network was applied separately to each group. For group1, thirty-four sets of data given in Table 1 were used to train the network and the five sets of data given in Table 4 were used to predict and validate the network. For Group 2, fifty-six sets of data given in Table 2 were used to train the network and the seven sets of data given in Table 5 were used to predict and validate the network.

As their orders of magnitude are different, before running the neural networks, the original data were normalized using Eq. (18) given below:

$$y_i = \frac{x_i - x_{\min}}{x_{\max} - x_{\min}} \tag{18}$$

In Eq. (18), x is the vector before normalization; y is the vector after normalization; x_i and y_i are respectively the element of vector x and vector y; $x_{\max}$ and $x_{\min}$ are respectively, the maximum and minimum element of vector x.

Several algorithms are available in the literature to train a neural network. Each of them has its advantages and disadvantages. For a given problem, it is difficult to say which one works best. It depends on several factors, such as the complexity of the problem, the number of training samples, the structure of the network, error target and so

Table 4
Prediction results of the 8 simulations for Group 1 (for $N=9$).

Blast no.	X_{50} (m)	X_{50R} (m)	X_{50K} (m)	X_{50N} (BP neural network) (m)									
				1	2	3	4	5	6	7	8	μ	δ
En13	0.47	0.39	0.44	0.39	0.42	0.42	0.42	0.42	0.42	0.42	0.42	0.42	0.0255
RU7	0.64	0.51	0.65	0.96	0.96	0.38	0.23	0.38	0.96	0.96	0.24	0.63	0.5571
Mg8	0.44	0.40	0.39	0.37	0.37	0.37	0.37	0.37	0.37	0.37	0.37	0.37	0.0000
Mg9	0.25	0.24	0.30	0.26	0.27	0.27	0.27	0.30	0.28	0.28	0.28	0.28	0.0430
Rc1	0.46	0.52	0.72	0.48	0.31	0.41	0.47	0.48	0.36	0.47	0.49	0.43	0.1544

X_{50}: Measured mean particle size (m), X_{50K}: Mean particle size based on Kuznetsov's equation (m), X_{50N}: Predicted mean particle size based on neural network model (m), X_{50R}: Mean particle size based on developed regression model (m).

Table 5
Prediction results of the 8 simulations for Group2 (for $N=7$).

Blast no.	X_{50} (m)	X_{50R} (m)	X_{50K} (m)	X_{50N} (BP neural network) (m)									
				1	2	3	4	5	6	7	8	μ	δ
Mr12	0.20	0.16	0.24	0.12	0.32	0.12	0.17	0.22	0.12	0.22	0.12	0.18	0.4093
Db10	0.35	0.16	0.08	0.17	0.28	0.16	0.17	0.20	0.74	0.20	0.74	0.33	0.7621
Sm8	0.18	0.19	0.35	0.19	0.19	0.19	0.19	0.19	0.19	0.19	0.19	0.19	0.0000
Oz8	0.23	0.17	0.20	0.18	0.14	0.14	0.12	0.13	0.15	0.13	0.15	0.14	0.1268
Oz9	0.17	0.16	0.23	0.19	0.19	0.18	0.22	0.19	0.17	0.19	0.17	0.19	0.0853
Ad23	0.21	0.18	0.11	0.22	0.19	0.23	0.17	0.22	0.22	0.22	0.22	0.21	0.0919
Ad24	0.20	0.14	0.13	0.19	0.21	0.19	0.17	0.25	0.23	0.25	0.23	0.22	0.1332

X_{50}: Measured mean particle size (m), X_{50K}: Mean particle size based on Kuznetsov's equation (m), X_{50N}: Predicted mean particle size based on neural network model (m), X_{50K}: Mean particle size based on developed regression model (m).

on. In this paper, the best training method was decided by trying different methods and observing the performance of each method on a plot between mean square error (*MSE*) value and number of training cycles. Four training methods: Levenberg–Marquardt (LM) algorithm, BFGS Quasi-Newton (BFGSQN) algorithm, Gradient Descent (GD) algorithm, and Gradient Descent Momentum (GDM) algorithm (Ge and Sun, 2007) were used to train the same selected network. The obtained results are shown in Fig. 3. It shows that the BFGS QN algorithm can provide results that are not stable and also it is subject to inaccuracies resulting from possible local minimum problems. In addition, the figure shows that the training speed of the BFGSQN algorithm is lower than that of the LM algorithm. The same figure shows that the training speed of the GD and GDM algorithms is much lower and their *MSE* values are much higher than that of the LM algorithm. That means the network performance of the GD and GDM algorithms is lower than that of the LM algorithm. It is also important to state that even though the plot of LM algorithm more or less remained the same with respect to different simulations, the plots of the remaining three algorithms changed significantly from one simulation to another. It indicates that the LM algorithm has the highest stability among the four training algorithms. Note that the LM algorithm has reached the global minimum after a few training cycles. The LM algorithm has been proposed by Hagan and Menhaj (He et al., 2005). The LM algorithm is an improved algorithm based on numerical optimization. Not only the first derivative information but also the second derivative information of the target function is used in the LM algorithm. It can dynamically adjust the convergence direction of iteration according to the iteration result, so its convergence speed is very fast (Wang et al., 2008). Fig. 3 shows that the LM algorithm is providing stable, very low *MSE* values at a low number of training cycles. This indicates that a network trained by the LM algorithm has good generalization ability and has the capability of providing good predictions compared to that of measured data. Therefore, from now onwards, the training of the neural networks that are discussed in the paper is performed using only the LM algorithm.

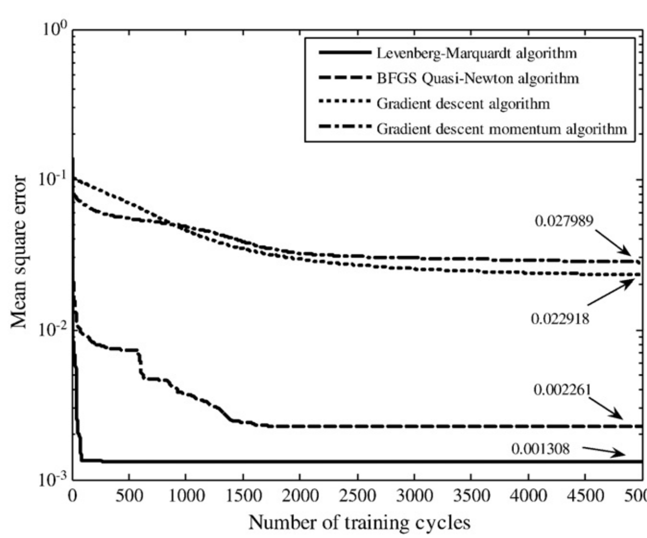

Fig. 3. Mean square error versus number of training cycles plot for the used training algorithms (Group 1 and $N=9$).

4.2. Influence of training sample size, number of weights and number of nodes on the accuracy of a trained network

For one hidden layer neural networks, Widrow (1987) and Baum and Haussler (1989) have suggested the equation $P=W/(1-a)$ as a necessary condition to relate *P*, the training sample size to a, the expected accuracy of the trained network and *W*, the number of weights to be trained. According to this equation, to obtain accuracies of 80% and 90% it is necessary to have a training sample of size$=5W$ and $10W$, respectively. In addition, Baum and Haussler (1989) have suggested the equation $P=(W/(1-a))$ $(\log\ nd/(1-a))$ as a sufficient condition to obtain an accuracy a, where nd is the number of nodes in the network. The latter condition increases the training sample size requirement further. On the other hand, Rogers and Dowla (1994) and Masters (1993) suggest the ratio between the number of training samples and the number of connection weights to be only 1and 2, respectively to obtain accurate trained networks. Due to the existence of such wide range opinion in the literature, Maier and Dandy (1998) performed an extensive investigation to study the effect of network geometry parameters on the network performance

Table 6
MSE values obtained for Group 1 at 500 learning cycles.

N value	Simulation no.							
	1	2	3	4	5	6	7	8
$N=6$	0.00140	0.00131	0.00131	0.00132	0.00535	0.00132	0.00132	0.00144
$N=7$	0.00131	0.00131	0.00132	0.00132	0.00133	0.00131	0.00132	0.00131
$N=8$	0.00131	0.00131	0.00131	0.00240	0.00131	0.00133	0.00132	0.00131
$N=9$	0.00131	0.00131	0.00134	0.00133	0.00131	0.00131	0.00132	0.00132
$N=10$	0.00133	0.00133	0.00132	0.00131	0.00131	0.00133	0.00132	0.00131

through a case study. Accuracy of the trained network was evaluated using the *MSE* value. They have obtained accurate results for neural networks having *P*/*W* in the range 0.36 to 2.14. They have also stated that the generalization ability of the trained network was not affected by using larger networks, despite the fact that limited training data were available. However, they have found network geometry to have an influence on training speed because the time taken to update the connection weights is a function of the number of weights. The above discussion indicates that no accepted rule is available to relate *P* to *W* and nd in forming network geometry for neural network analysis. The authors feel that one of the best practical ways to evaluate the accuracy of the trained networks is through calculation of *MSE*. That is the approach used in this paper.

Tables 6 and 7 show the *MSE* values obtained during training for Groups 1 and 2 data, respectively at 500 learning cycles using the LM algorithm for different number of hidden layers *N* and for different simulations. Note that the optimum *N* obtained for Groups 1 and 2 are 9 and 7, respectively (see Section 4.3). *MSE* values appearing in Tables 6 and 7 indicate high accuracy of trained networks. Note that the trained networks obtained for different *N* and different simulations are used to make predictions and to evaluate the accuracy of predictions in Section 4.3. For Groups 1 and 2, *MSE* ranges of 1.31–1.34×10^{-3} and 2.6–2.7×10^{-4}, respectively have been obtained for optimum *N*. For Group 1, in the training sample, En3 and En5, En8 and En9, En11 and En12 had the same values of *S*/*B*, *H*/*B*, *B*/*D*, *T*/*B*, Pf, X_B and *E*. However, their values of X_{50} were not the same (see Table 1). Mg5 and Mg7 had the same values of *S*/*B*, *H*/*B*, *B*/*D*, *T*/*B*, Pf, *E* and X_{50}. However, their value of X_B was not the same (see Table 1). Due to the above reasons, the training precision of Group1 was slightly lower than that for Group 2.

4.3. Procedure to estimate number of units for the hidden layer

Choosing an appropriate number for the units in the hidden layer is not a straightforward task (Maier and Dandy, 1997). The number of input parameters, number of output parameters, number of data sets available and the characteristics of the functional relation between the output and the input parameters may affect the optimum number for the units in the hidden layer. At present, the authors are not aware of any accepted procedure or formula available to determine the aforesaid optimum number. This optimum number may even change with different run (simulation) numbers for the same problem. Two empirical formulae available in the literature are used in this paper to estimate the optimum number for the hidden layer units.

Based on Kolmogorov's theorem, Hecht-Nelson (1987) has suggested that 2n+1 (where *n* is the number of input parameters) should be used as the upper bound for the number of hidden units for a one-hidden-layer back-propagation network. Because in our study $n=7$, the number of hidden units for both Groups1 and 2 should be ≤ 15 according to Hecht-Nelson's suggestion. According to the second empirical formula (Ge and Sun, 2007), the number of hidden units, *N*, should satisfy the following inequality:

$$\sum_{i=0}^{n} C_N^i > k \tag{19a}$$

where

$$C_N^i = \frac{N!}{i!(N-i)!} \tag{19b}$$

In inequality (19a), *n* is the number of input parameters and *k* is the number of data sets used. Note that If $i>N$, $C_N^i=0$. Application of inequality (19a) to Group 1 ($n=7$, $k=34$) and Group 2 ($n=7$, $k=56$) results in $N\geq6$ for both groups. Therefore, use of the aforementioned two empirical criteria results in $6\leq N\leq15$ for both Groups 1 and 2.

Accuracy of the network was considered to determine the optimum value for *N*. To evaluate the accuracy of the network for each *N*, two parameters were used. The Root Mean Square Error, *RMSE*, was used as the first parameter and it was defined by the following equation:

$$RMSE_i = \sqrt{\frac{\sum_{j=1}^{J} error_{ij}^2}{J}} \tag{20a}$$

where

$$error_{ij} = |e_{ij}-r_{ij}| \tag{20b}$$

In Eq. (20b), e_{ij} denotes the prediction result of the *i*th network under a certain *N* for the *j*th blast number, r_{ij} denotes the corresponding actual value for the same blast number. In Eq. (20a), *J* is the number of blast data used for prediction for a certain group. The correlation coefficient between the predicted value and the measured value for the aforementioned *J* blast data was used as the second parameter to evaluate the accuracy of each *i*th network under a certain *N* value. In evaluating the accuracy, several random simulations were performed for each *i*th network under a certain *N* value.

4.4. Results, prediction and validation

For Group 1, five blasts were used for the prediction and validation. Note that under each *N* value, 8 simulations were made. As an example, the prediction obtained for each blast under $N=9$ for each of the simulations made is shown in Table 4. En13 blast has the same values of *S*/*B*, *H*/*B*, *B*/*D*, *T*/*B*, Pf, X_B and *E* as for En4 blast. Therefore, the prediction result of X_{50} for En13 blast is almost the same as the value for En4 blast. For RU7 and RU1, all the blasting parameter values are the same apart from the value for *T*/*B*. That has led to a large variation of the predicted value with respect to the simulation number. Table 4 also provides the predicted mean, μ, and coefficient of variation, δ, obtained for each blast from the 8 simulations.

The *RMSE* values and the coefficient of variations obtained for Group 1 for different *N* values are given in Table 8. High correlation coefficient values indicate predictions close to the measured values. The consistency of the correlation coefficient values shows high homogeneity of the Group 1 samples. $N=9$ has resulted in the lowest *RMSE* and the highest correlation coefficient. That means for Group 1, $N=9$ is the optimum value. Table 4 shows a comparison between

Table 7
MSE values obtained for Group 2 at 500 learning cycles.

N value	Simulation no.							
	1	2	3	4	5	6	7	8
$N=6$	0.00031	0.00027	0.00026	0.00026	0.00026	0.00026	0.00026	0.00026
$N=7$	0.00026	0.00026	0.00026	0.00026	0.00026	0.00026	0.00027	0.00027
$N=8$	0.00026	0.00026	0.00026	0.00026	0.00026	0.00054	0.00027	0.00026

Table 8
Prediction results of mean particle size from ANNA for Group1 (for $N = 6–15$).

Blast no.		En13	RU7	Mg8	Mg9	Rc1	Correlation coefficient (with X_{50})	*RMSE*
X_{50} (m)		0.47	0.64	0.44	0.25	0.46	1.00	
$N = 6$	μ	0.42	0.86	0.37	0.27	0.40	0.90	0.1093
	δ	0.0169	0.1595	0.0079	0.0479	0.3480		
$N = 7$	μ	0.42	0.56	0.37	0.27	0.54	0.88	0.0642
	δ	0.0275	0.5837	0.0127	0.0410	0.4018		
$N = 8$	μ	0.42	0.74	0.37	0.28	0.51	0.93	0.0645
	δ	0.0000	0.4460	0.0056	0.0698	0.3098		
$N = 9$	μ	0.42	0.63	0.37	0.28	0.43	0.96	0.0429
	δ	0.0284	0.5553	0.0071	0.0275	0.1549		
$N = 10$	μ	0.42	0.64	0.37	0.27	0.58	0.87	0.0666
	δ	0.0003	0.5480	0.0031	0.0249	0.2648		
$N = 11$	μ	0.42	0.78	0.37	0.28	0.60	0.89	0.0974
	δ	0.0146	0.4193	0.0036	0.0272	0.1477		
$N = 12$	μ	0.42	0.61	0.37	0.28	0.39	0.94	0.0531
	δ	0.0000	0.5691	0.0069	0.0584	0.2199		
$N = 13$	μ	0.42	0.67	0.37	0.28	0.46	0.95	0.0431
	δ	0.0000	0.5472	0.0065	0.0488	0.3262		
$N = 14$	μ	0.42	0.60	0.37	0.27	0.55	0.77	0.0592
	δ	0.0000	0.5611	0.0019	0.0420	0.1954		
$N = 15$	μ	0.42	0.74	0.37	0.26	0.54	0.93	0.0691
	δ	0.0000	0.4175	0.0000	0.0602	0.2556		

X_{50}: Measured mean particle size (m).

neural network predictions, measured values and predictions based on the Kuznetsov's equation. All the blast data were examined carefully and the rock factor ‘A’ was estimated for each blast to apply the Kuznetsov's equation. For all 5 blasts, neural network predictions are close to the measured values. This can be also seen from the regression analysis results given in Fig. 4a. For 4 out of the 5 blasts, predictions based on Kuznetsov's equation are close to the measured values. This can be also seen from the regression analysis results given in Fig. 4b. Note that Group 1 blast data come from hard rocks that have high elastic modulus values.

For Group 2, seven blasts were used for the prediction and validation. Note that under each N value, 8 simulations were made. As an example, the prediction obtained for each blast under $N = 7$ for each of the simulations made is shown in Table 5. The same table also provides the predicted mean, μ, and coefficient of variation, δ, obtained for each blast from the 8 simulations. The *RMSE* values and the coefficient of variations obtained for Group 2 for different N values are given in Table 9. The results show high fluctuation of correlation coefficient values for Group 2 data. This shows that the homogeneity of Group 2 is weaker than that of Group 1. $N = 7$ has resulted in the lowest *RMSE* value and the highest correlation coefficient. That means for Group 2, $N = 7$ is the optimum value. Table 5 shows a comparison between neural network predictions, measured values and predictions based on the Kuznetsov's equation. For all 7 blasts, neural network predictions are close to the measured values. This can be also seen from the regression analysis results given in Fig. 4a. Only for about 50% of the blasts, predictions based on Kuznetsov's equation are close to the measured values. This can be also seen from the regression analysis results given in Fig. 4b. Note that Group 2 blast data come from rocks that have relatively low elastic modulus values.

Fig. 4a shows the linear regression analysis performed between the predictions obtained from the neural network models developed for Groups 1 and 2 and the measured mean particle size. Fig. 4b shows the linear regression analysis performed between the predictions based on Kuznetsov's equation for Groups 1 and 2 and the measured mean particle size. In Fig. 4a, the prediction line has an intercept close to zero and a slope close to 1.0 with a R^2 value of 0.9407 (which indicates a strong regression fit). These results indicate that the matching between the neural network predictions and the measured values is very strong. In Fig. 4b, even though the prediction line has an intercept close to zero and a slope close to 1.0, the R^2 value is only

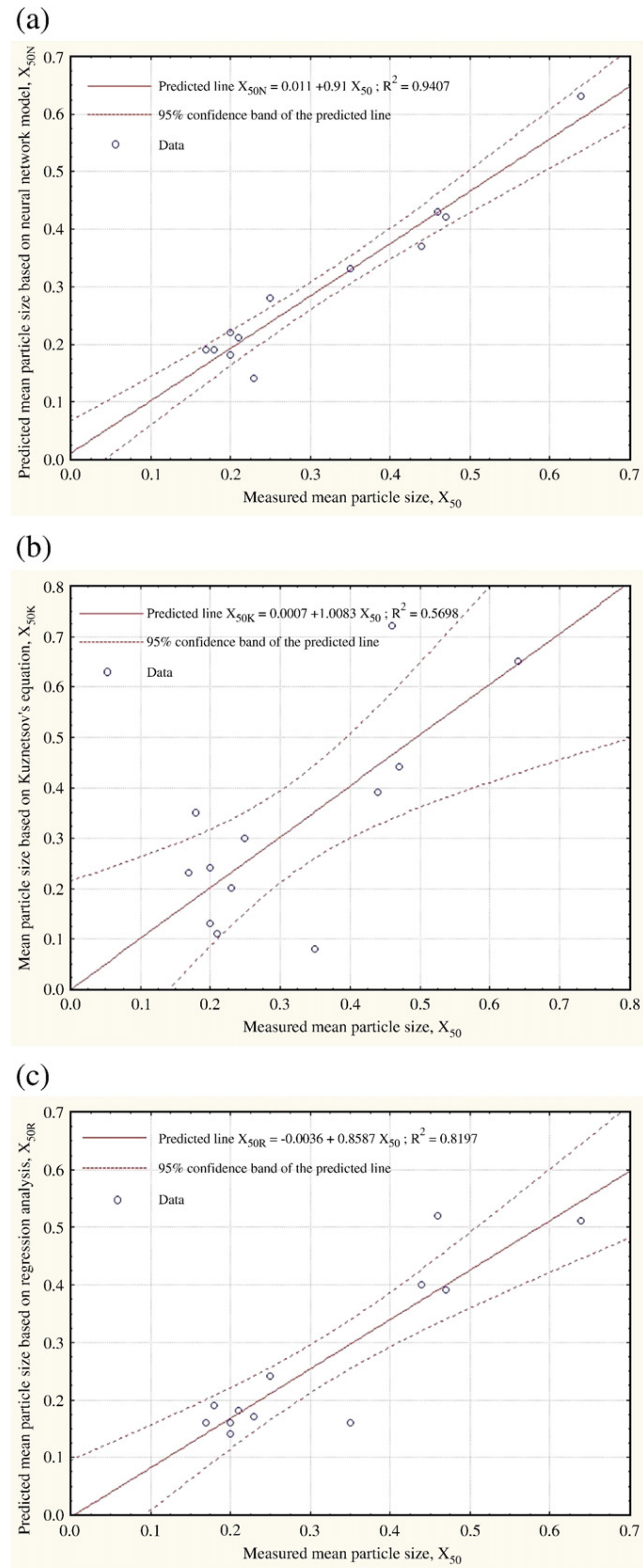

Fig. 4. Predicted mean particle size (m) versus measured mean particle size (m): (a) Based on neural network models; (b) based on Kuznetsov's equation; and (c) based on developed regression models.

0.5697 (which indicates only a moderate level regression fit). In addition, the 95% confidence band in Fig. 4a is much narrower than that in Fig. 4b. These results clearly show that the neural network predictions are better than the predictions based on Kuznetsov's equation.

Table 9
Prediction results of mean particle size from ANNA for Group2 (for $N=6$–15).

Blast no.		Mr12	Db10	Sm8	Oz8	Oz9	Ad23	Ad24	Correlation coefficient (with X_{50})	*RMSE*
X_{50} (m)		0.20	0.35	0.18	0.23	0.17	0.21	0.20	1.00	
$N=6$	μ	0.19	0.19	0.18	0.14	0.17	0.20	0.19	0.11	0.0834
	δ	0.5159	0.5700	0.1365	0.1059	0.1287	0.2082	0.1551		
$N=7$	μ	0.18	0.33	0.19	0.14	0.19	0.21	0.22	0.81	0.0425
	δ	0.4093	0.7621	0.0000	0.1268	0.0853	0.0919	0.1332		
$N=8$	μ	0.28	0.30	0.19	0.14	0.21	0.25	0.20	0.49	0.0640
	δ	0.8467	0.8615	0.0005	0.0322	0.3374	0.3733	0.0956		
$N=9$	μ	0.41	0.43	0.19	0.14	0.20	0.29	0.20	0.59	0.1136
	δ	0.6653	0.6185	0.0000	0.0495	0.0832	0.6729	0.0409		
$N=10$	μ	0.33	0.33	0.19	0.14	0.19	0.26	0.20	0.52	0.0767
	δ	0.7884	0.7237	0.0000	0.0089	0.3196	0.3535	0.1177		
$N=11$	μ	0.31	0.35	0.17	0.13	0.16	0.19	0.19	0.68	0.0671
	δ	0.7188	0.7518	0.1878	0.0681	0.1654	0.2405	0.2480		
$N=12$	μ	0.31	0.45	0.19	0.14	0.18	0.29	0.22	0.78	0.0865
	δ	0.7063	0.6182	0.0000	0.0060	0.1346	0.4057	0.1344		
$N=13$	μ	0.39	0.36	0.19	0.14	0.17	0.23	0.20	0.49	0.0951
	δ	0.7322	0.6801	0.0000	0.0050	0.1009	0.1552	0.0909		
$N=14$	μ	0.39	0.38	0.18	0.14	0.16	0.21	0.19	0.57	0.0955
	δ	0.6019	0.7096	0.1361	0.0714	0.1654	0.2076	0.1746		
$N=15$	μ	0.21	0.30	0.18	0.14	0.17	0.20	0.19	0.79	0.0484
	δ	0.6902	0.6597	0.1365	0.0545	0.1518	0.1937	0.1562		

X_{50}: Measured mean particle size (m).

5. Prediction of mean particle size based on multivariate regression analysis

The multiple regression analysis (Draper and Smith, 1981) was applied to develop a prediction equation for each group. The dependent variable of the multiple regression analysis is the mean particle size (x_{50R}) and the independent variables are the all blast design parameters, elastic modulus and in-situ block size.

Eq. (21) given below was developed for Group 1 that has high Young's modulus values. Table 10 shows the obtained regression statistics.

$$X_{50} = 208.(S/B)^{2.788}.(H/B)^{0.112}.(B/D)^{0.027}.(T/B)^{-0.321}.(Pf)^{-0.360}.(X_B)^{0.233}.(E)^{-1.802} \tag{21}$$

R, the multiple correlation coefficient, is the linear correlation between the observed and model-predicted values of the dependent variable. Its large value (close to 1) indicates a strong relation. R^2, the coefficient of determination, is the squared value of the multiple correlation coefficient. R^2 is the percent of variance in the dependent variable explained collectively by all of the independent variables. R^2 value close to 1 also indicates importance of regression. The regression row in Tables 10 and 11 provide information about the variation accounted by the regression model. The residual row displays information about the variation that is not explained by the regression model (Draper and Smith, 1981; Montgomery et al., 2006). For example, the sum of squares values given in Table 10 show that over 70% of the variance in the mean particle size (x_{50R}) is explained by the regression model. The *F* test is applied to test the significance of the regression model. If the significance value of the *F* statistic is less than 0.05, it means that the variation explained by the model is not due to chance. In other words, the null hypothesis of no linear relationship of x_{50R} to the 7 independent variables is rejected. Table 10 shows a significance value of very close to zero based on the *F* and the degrees of freedom (*df*) value calculated. That indicates the importance of the developed regression equation for Group 1.

The equation given below was developed for Group 2 that has low elastic modulus values. Table 11 shows the regression statistics obtained for Eq. (22). Slightly higher R^2 and *R* values were obtained for Group 2 in comparison to Group 1. Again a significance value of very close to zero was obtained under ANOVA results. All these values indicate that the regression is important and strong for Group 2.

$$X_{50} = 3.34.(S/B)^{0.073}.(H/B)^{0.644}.(B/D)^{-0.150}.(T/B)^{-0.349}.(Pf)^{-0.155}.(X_B)^{0.130}.(E)^{-1.159} \tag{22}$$

The coefficients associated with the modulus of elasticity are negative for Eqs. (21) and (22). Increase of the elastic modulus results in decrease of the mean particle size. The modulus of elasticity is an indicator of rock stiffness. In the developed models, if the stiffness of rock increases the fragmentability of rock increases.

Table 10
Regression statistics obtained for Eq. (21).

Model summary				
R	R^2	Adjusted R^2	Standard error	Observations
0.841	0.708	0.632	0.0916	35

Analysis of variance (ANOVA)					
	Sum of squares	*df*	Mean square	*F*	Significance
Regression	0.551	7	0.079	9.356	0.000
Residual	0.227	27	0.008		
Total	0.778	34			

Table 11
Regression statistics obtained for Eq. (22).

Model summary					
R	R^2	Adjusted R^2	Standard error		Observations
0.806	0.649	0.598	0.1046		56
Analysis of variance (ANOVA)					
	Sum of squares	df	Mean square	F	Significance
Regression	0.972	7	0.139	12.684	0.000
Residual	0.525	48	0.011		
Total	1.497	55			

Eqs. (21) and (22) were applied respectively, to the 5 blasts shown in Table 4 and the 7 blasts shown in Table 5 to predict mean particle size based on the developed regression equations. The values obtained are shown in Tables 4 and 5, respectively. For all 5 blasts belonging to Group 1, the regression based predictions are close to the measured values. For the 7 blasts belonging to Group 2, apart from DB10, for the rest, the regression based predictions are close to the measured values. Fig. 4c shows the regression analysis performed between the predictions based on the regression equation and the measured mean particle size. Even though the intercept of the prediction line is almost zero, the slope (equal to 0.86) is slightly off from 1.0. However, the R^2 value of 0.82 indicates a strong regression fit and the 95% confidence band is much tighter than the one appears in Fig. 4b. Comparison of Fig. 4b and c shows that the regression based predictions have better reliability than the predictions based on Kuznetsov's equation. Comparison of Fig. 4a and c shows that the neural network predictions are better than the predictions based on developed multivariate regression models.

6. Discussion

Note that even though both the multivariate regression models and neural network models are non-linear models, the neural network models can be considered as more advanced non-linear models than multivariate regression models. It is important to note that neural network results do not provide a unique answer. The results depend on the factors such as network geometry, internal parameters of the learning algorithm and the simulation number. The deviation associated with the simulation number can be reduced by computing the mean value coming out of several simulations as done in this paper. For engineering and science problems, it is an extremely difficult task to find large data bases. Therefore, as shown in this paper, attempts should be made to find the optimum network geometry and the best learning algorithm to obtain the best possible results for problems having a limited number of data. Best learning algorithms can be obtained as shown in the paper through numerical experimentation to minimize the *MSE* between the predicted value and the expected value and to maximize the training speed and the stability of the calculated *MSE* with number of training cycles. There is no universally accepted theoretical basis for choosing the network geometry. Therefore, in practical use, it should be obtained through numerical experimentation as shown in the paper to minimize the *RMSE* obtained between the prediction and the measured value. This will increase the workload when using the neural network approach. The learning and memory ability of a neural network depend on the training samples used. Therefore, if new data become available, to obtain accurate predictions, the network has to be rebuilt again from the very beginning.

7. Conclusions

In a previous paper by three of the authors of this paper (Hudaverdi et al., 2010), many blasts performed in different parts of the world and reported in the literature were put together to create a blast data base to develop fragmentation distribution models. In the same paper, a hierarchical cluster analysis was used to separate the blasts data into two different groups of similarity based on the intact rock stiffness. In the same study the group memberships obtained from cluster analysis was confirmed by a discriminant analysis. A part of this blast data was used in this study to train a single-hidden layer back-propagation neural network model to predict mean particle size resulting from blast fragmentation for each of the obtained similarity groups. The mean particle size was considered to be a function of seven independent parameters. It turned out to be a difficult assignment to find common intact rock and rock mass parameters for all the selected blast data to use in developing fragmentation distribution models. On the other hand, it was possible to find in-situ block size for all the blasts in the data base. Therefore, in-situ block size which is accepted as one of the key parameters of the fragmentation process was used to represent rock mass structure in the developed models. With respect to intact rock, the modulus of elasticity turned out to be the most common parameter available for all the blasts and was used to represent intact rock properties in the developed models. Consequently, two rock parameters which are widely used in the literature related to blast fragmentation were included in the fragmentation prediction models. It was possible to incorporate most of the important blast design parameters in the developed models.

Four learning algorithms were considered to train neural network models. Levenberg–Marquardt algorithm turned out to be the best one providing the highest stability and maximum learning speed. An extensive analysis was performed to estimate the optimum value for the number of units for the hidden layer. The blast data that were not used for training were used to validate the trained neural network models. Capability of the developed neural network models was determined by comparing neural network predictions with measured mean particle size and the predictions based on one of the most applied fragmentation prediction models appearing in the blasting literature. Prediction capability of the trained neural network models was found to be strong and better than the most applied fragmentation prediction model. For the same two similarity groups, multivariate regression models were also developed to predict mean particle size. The prediction capability of the multivariate regression models was also found to be strong and better than the most applied fragmentation prediction model. The prediction capability of the neural network models seems to be superior to that of multivariate regression models for the used data. No other study reported in the literature has used a large data base as that used in this study. Therefore, the diversity of the blasts data base is one of the strongest features of the developed models. The variety of the blasts is also an important element that increases the versatility and reliability of the developed models. The developed neural network models as well as multivariate regression models are not complex and are suitable for practical use at mines. As a result of this study, two different neural network models and two different multivariate regression models were developed to predict mean particle size resulting from blasting. This provides an opportunity to use a different prediction model in accordance with the value of modulus of elasticity of intact rock.

Researchers use different procedures in estimating in-situ block size. A wide variation is possible for the determination technique of the in-situ block size. In the future, attempts should be made to provide uniformity in estimating the in-situ block size to increase accuracy. At present, the developed models incorporate elastic modulus to represent the intact rock. In the future, attempts may be made to determine additional rock parameters of the rock mass that would be subjected to blasting. Application of the developed prediction models to new blasts will test the reliability of them. Attempts should be made to enlarge the blast database that will be used to develop fragmentation prediction models presented in this study. Neural network and multivariate statistical modeling procedures used in this paper have shown the capability of developing accurate fragmentation prediction models.

Acknowledgements

This study was partially supported by the Research Fund of the Istanbul Technical University (project name: ‘the investigation of environmentally friendly blast designs for improvement of fragmentation in Istanbul region quarries’). The authors are grateful to the Research Fund of the Istanbul Technical University for their financial support.

References

Aler, J., Du Mouza, J., Arnould, M., 1996. Measurement of the fragmentation efficiency of rock mass blasting and its mining applications. International Journal of Rock Mechanics and Mining Sciences and Geomechanics Abstracts 33, 125–139.

Al-Kaabl, A.U., Lee, W.J., 1993. Using artificial neural nets to identify the well-test interpretation model. SPE Formation Evaluation 8, 233–240.

Ash, R.L., 1963. The mechanics of the rock breakage (Part 1). Pit and Quarry 56 (2), 98–100.

Baum, E.B., Haussler, D., 1989. What size net gives valid generalization? Neural Computation 1, 151–160.

Castro, J.T., Liste, A.V., Gonzalez, A.S., 1998. Blasting Index for Exploitation of Aggregates. In: Singhhal, R.K. (Ed.), Proceedings of the 7. Mine Planning and Equipment Selection Symposium, Calgary, Canada, pp. 165–168.

Chakraborty, A.K., Jethwa, J.L., Paithankar, A.G., 1994. Effects of joint orientation and rock mass quality on tunnel blasting. Engineering Geology 37, 247–262.

Chakraborty, A.K., Raina, A.K., Ramulu, M., Choudhury, P.B., Haldar, A., Sahu, P., Bandopadhyay, C., 2004. Parametric study to develop guidelines for blast fragmentation improvement in jointed and massive formations. Engineering Geology 73, 105–116.

Cunningham, C.V.B., 1983. The KuzRam Model for Prediction of Fragmentation from Blasting. In: Holmberg, R., Rustan, A. (Eds.), Proceedings of 1. International Symposium on Rock Fragmentation by Blasting, Lulea, Sweden, pp. 439–453.

Cunningham, C.V.B., 1987. Fragmentation Estimations and KuzRam Model—Four Years On. Proceedings of 2. Int. Symposium on Rock Fragmentation by Blasting, Keystone, Colorado, pp. 475–487.

Cybenko, G., 1989. Approximation by superpositions of a sigmoidal function. Mathematical Control Systems and Signaling 2, 303–314.

De Groot, P.F.M., 1993. Reservoir characterization from 3-D seismic data using artificial neural networks and stochastic modeling techniques. AAPG Bull 77, 1617–1618.

Draper, N.R., Smith Jr., H., 1981. Applied Regression Analysis, 2nd ed. John Wiley and Sons, Inc., New York, N.Y.

Eberhart, R.C., Dobbins, R.W., 1990. Neural Network PC Tools. Academic Press, London. 414 pp.

Ge, Z.X., Sun, Z.Q., 2007. Neural network theory and MATLAB R2007 application. Publishing House of Electronics Industry, Beijing, 108–122p, 48–50p.

Ghaboussi, J., 1992. Potential Applications of Neuro-biological Computational Models in Geotechnical Engineering. Proc. Fourth Int. Symp. on Numerical Models in Geotechnics, Swansea, U.K, pp. 543–555.

Gheibie, S., Aghababaei, H., Hoseinie, S.H., Pourrahimian, Y., 2009. Modified Kuz–Ram fragmentation model and its use at the Sungun Copper Mine. International Journal of Rock Mechanics & Mining Sciences 46, 967–973.

Ghosh, A., Daemen, J.J.K., Vanzyl, D., 1990. Fractal Based Approach to Determine the Effect of Discontinuities on Blast Fragmentation. Proc. of the 31st U.S. Symp. on Rock Mechanics, Golden, pp. 905–912.

Grundstrom, C., Kanchibotla, S., Jankovic, A., Thornton, D.M., 2001. Blast Fragmentation for Maximizing the SAG Mill Throughput at Porgera Goldmine. Proceedings of the 27. Annual Conference on Explosives and Blasting Technique, Orlando, Florida, pp. 383–399.

Hagan, T.N., 1995. The effect of rock properties on the design and results of tunnel blasts. Journal of Rock Mechanics and Tunnelling Technology 1 (1), 25–39.

Hall, J., Brunton, I., 2002. Critical comparison of Kruttschnitt Mineral Research Center (JKMRC) blast fragmentation models. Fragblast 6 (2), 207–220.

Hamdi, E., Du Mouza, J., 2005. A methodology for rock mass characterization and classification to improve blast results. International Journal of Rock Mechanics & Mining Sciences 42, 177–194.

Hamdi, E., Du Mouza, J., Fleurisson, J.A., 2001. Evaluation of the part of blasting energy used for rock mass fragmentation. Fragblast 5 (3), 180–193.

He, X.Z., Zhang, X.P., Zhang, S.J., 2005. Improved L–M algorithm for ANNs prediction of phase equilibrium in macromolecule system. Journal of Chemical Industry and Engineering 56 (3), 392–399.

Hecht-Nelson, R., 1987. Kolmogorov's Mapping Neural Network Existence Theorem. Proc. of 1st IEEE Annual Int'l Conf. on Neural Networks, San Diego. IEEE Press, Piscataway, NJ, p. III: 11-14. June 21–24.

Hjelmberg, H., 1983. Some İdeas on How to İmprove Calculations of the Fragment Size Distribution in Bench Blasting. 1st International Symposium on Rock Fragmentation by Blasting. Lulea University Technology Lulea, Sweden, pp. 469–494. Aug. 22–26.

Hudaverdi, T., 2004. The investigation of the optimum parameters in large scale blasting at KBI Black Sea Copper Works — Murgul open-pit mine (in Turkish). MSc Thesis, Istanbul Technical University, Institute of Science and Technology, pp. 45–67.

Hudaverdi, T., Kulatilake, P.H.S.W., Kuzu, C., 2010. Prediction of Blast Fragmentation Using Multivariate Analysis Procedures. To appear in 2010.

Hustrulid, W., 1999. Blasting Principles for Open Pit Mining. A.A. Balkema, Rotterdam.

Jhanwar, J.C., Jethwa, J.L., Reddy, A.H., 2000. Influence of air-deck blasting on fragmentation in jointed rocks in an open-pit manganese mine. Engineering Geology 57, 13–29.

Kanchibotla, S.S., Valery, W., Morrell, S., 1999. Modeling Fines in Blast Fragmentation and Its Impact on Crushing and Grinding. Proceedings of the Explo-99 Conference, Kalgoorlie, Australia, pp. 137–144.

Khaw, John F.C., Lim, B.S., Lim, Lennie E.N., 1995. Optimal design of neural networks using the Taguchi method. Neurocomputing 7, 225–245.

Kou, S., Rustan, A., 1993. Computerized Design and Result Prediction of Bench Blasting. Proceedings of the Fourth International Symposium on Rock Fragmentation by Blasting, Vienna, pp. 263–271.

Kung, T.C., Hsiao, C.L., Schuster, M., Juang, C.H., 2007. A neural network approach to estimating excavation-induced wall deflection in soft clays. Computers and Geotechnics 34, 385–396.

Kuznetsov, V.M., 1973. Mean diameter of fragments formed by blasting rock. Soviet Mining Science 9 (2), 144–148.

Latham, J.P., Lu, P., 1999. Development of an assessment system for the blastability of rock masses. International Journal of Rock Mechanics and Mining Sciences and Geomechanics Abstracts 36, 41–55.

Latham, J.P., Kemeny, J., Maerz, N., Noy, M., Schleifer, J., Tose, S., 2003. A blind comparison between results of four image analysis systems using a photo-library of piles of sieved fragments. Fragblast 7 (2), 105–132.

Lee, C., Sterling, R., 1992. Identifying probable failure modes for underground openings using a neural network. International Journal of Rock Mechanics and Mining Sciences 29 (1), 49–67.

Li, Q., Yu, J.Y., Mu, B.C., Sun, X.D., 2006. BP neural network prediction of the mechanical properties of porous NiTi shape memory alloy prepared by thermal explosion reaction. Material Science and Engineering, A 419, 214–217.

Lilly, P.A., 1986. An Empirical Method of Assessing Rock Mass Blastability. Proc. Large Open Pit Conference, IMM, Australia, pp. 89–92.

Maier, H.R., Dandy, G.C., 1997. The effect of internal parameters and geometry on the performance of back-propagation neural networks: an empirical study. Environmental Modeling & Software 13, 193–209.

Maier, H.R., Dandy, G.C., 1998. The effect of internal parameters and geometry on the performance of back-propagation neural networks: an empirical study. Environmental Modelling & Software 13, 193–209.

Masters, T., 1993. Practical Neural Network Recipes in C ++. Academic Press, San Diego.

Mckenzie, A.S., 1966. Cost of explosives—do you evaluate it properly? Mining Congress Journal 52 (5), 32–41.

Mojtabai, N., Farmer, I.W., Savely, J.P., 1990. Optimisation of Rock Fragmentation in Bench Blasting. Proc. 31st US Symposium on Rock Mechanics. Balkema, Rotterdam, pp. 897–901.

Montgomery, D.C., Peck, E.A., Vining, G.G., 2006. Introduction to Linear Regression Analysis. John Wiley & Sons Inc, New Jersey, USA.

Nie, S.-L., Rustan, A., 1987. Techniques and Procedures in Analyzing Fragmentation after Blasting by Photographic Method. Proc. 2nd International Symposium on Rock Fragmentation by Blasting, Keystone, Colorado, pp. 36–47.

Ouchterlony, F., Niklasson, B., Abrahamsson, S., 1990. Fragmentation monitoring of production blasts at Mrica. In: McKenzie, C. (Ed.), International Symposium on Rock Fragmentation by Blasting, FragBlast 3. Brisbane, Australia, pp. 283–289.

Ozcelik, Y., 1998. Effect of discontinuities on fragment size distribution in open-pit blasting — a case study. Transactions of the Institution of Mining and Metallurgy 107, 146–150.

Pal Roy, P., 1995. Breakage assessment through cluster analysis of joint set orientations of exposed benches of opencast mines. Geotechnical and Geological Engineering 13, 79–92.

Penn, B.S., Gordon, A.J., Wendlandt, R.F., 1993. Using neural networks to locate edges and linear features in satellite images. Computers & Geosciences 19, 1545–1565.

Rizzo, D.M., Doughery, D.E., 1994. Characterization of aquifer properties using artificial neural networks; neural kriging. Water Resources Research 30, 483–497.

Rogers, L.L., Dowla, F.U., 1994. Optimization of groundwater remediation using artificial neural networks with parallel solute transport modeling. Water Resources Research 30, 457–481.
Rogers, S.J., Fang, J.H., Karr, C.L., Stanley, D.A., 1992. Determination of lithology from well logs using a neural network. AAPG Bull 76, 731–739.
Rosin, P., Rammler, E., 1933. The laws governing the fineness of powdered coal. Journal of the Institute of Fuel 7, 29–36.
Rustan, P.A., 1998. Automatic Image Processing and Analysis of Rock Fragmentation—Comparison of Systems and New Guidelines for Testing the Systems. The International Journal for Blasting and Fragmentation. Fragblast, vol. 2, (1). Balkema, Rotterdam, pp. 15–23.
Sanchidrian, J.A., Segarra, P., Lopez, L.M., 2007. Energy components in rock blasting. International Journal of Rock Mechanics & Mining Sciences 44, 130–147.
Schuhmann Jr., R., 1959. Energy input and size distribution in comminution. Am. Inst. Min. Metall., AIME, 214, 22–25.
Thomas, A.L., La Pointe, P.R., 1995. Conductive Fracture Identification Using Neural Networks. Proc. 36th US Symp. on Rock Mech. Balkema, Rotterdam, pp. 627–632.
Tung, A.T.Y., Wong, F.S., Dong, W., 1994. Prediction of the spatial distribution of the modified Mercalli intensity using neural networks. Journal of Earthquake Engineering and Structural Dynamics 23, 49–62.
Wang, K.L., Yang, L., Zha, F.G., 2008. The application of BP neural network in evaluating enterprise network marketing performance. Commercial Research 371, 64–68.
Widrow, B., 1987. ADALINE and MADALINE — 1963, Plenary Speech. Proc. IEEE 1st Int. Conf. on Neural Networks, San Diego, CA, Vol. I, pp. 143–158.
Yu, S.W., Zhu, K.J., Diao, F.Q., 2008. A dynamic all parameters adaptive BP neural networks model and its application on oil reservoir prediction. Applied Mathematics and Computation 195, 66–75.
Zhang, Q., Song, J.R., Nie, X.Y., 1991. The application of neural network to rock mechanics and rock engineering. International Journal of Rock Mechanics and Mining Sciences 28, 535–540.
Zhang, L., Luo, J.H., Yang, S.Y., 2009. Forecasting box office revenue of movies with BP neural network. Expert Systems with Applications 36, 6580–6587.